CrystEngComm

Accepted Manuscript

ROYAL SOCIETY OF CHEMISTRY

www.rsc.org/crystengcomm

CrystEngComm RSCPublishing

ARTICLE

Peculiar Phenomena on Structural Transformation Triggered from A Nickel Coordination Polymer†

Cite this: DOI: 10.1039/x0xx00000x

Meng Kang, Guo-Ping Yang, Lei Hou, Wei-Ping Wu, Yun-Long Wu and Yao-Yu Wang*

Received 00th January 2012,
Accepted 00th January 2012

DOI: 10.1039/x0xx00000x

www.rsc.org/

Structural transformation has aroused wide concern and emerged as a promising approach for the design and synthesis of novel coordination polymers. In this work, we found the interesting phenomena on the structural transformation triggered from a nickel coordination polymer (CP). Two temperature-dependent two-dimensional (2D) CPs, **1** and **2** were synthesized by hydrothermal reaction, while the other two CPs, 2D **3** and 3D **4** were prepared by in-situ thermal decomposition of **1**. Interestingly, **1** could undergo methanol-mediated transformation to afford **2** and **2** might convert to **1** under the condition of adding bipy in water. The multistep conversions from **1** to **3** and **3** to **4** triggered by heat treatment in the solid state accompany a very scarce dynamic response of sequential release of coordinated water and partial organic ligands. More importantly, the mechanism of the transformation has also been studied in details. Moreover, **3** could revert back to **1** quickly upon exposure in air, and this reversible process of dehydration-rehydration could be repeated at least ten times, which could highlight their application in the sensors of moisture.

Introduction

Over the past decades, substantial interesting coordination polymers (CPs) have been prepared via traditional hydro/solvo-thermal synthesis.[1] Even so, there is no sufficient information on the possible ways for the formation of coordination networks.[2] As a result, structural transformation has aroused wide concern and emerged as a promising approach for the design and synthesis of novel CPs, since it provides some crucial clues to gain intensive understanding on the fundamental external stimuli: temperature,[3] mechanical force,[4] solution,[5] reaction time,[6] guest molecule[7] and electromagnetic irradiation.[8] Moreover, CPs that show reversible structure transformation and a characteristic response toward specific external stimuli are vitally important for applications in sensing, molecular capture, switch, and so on.[9]

Generally, the structural transformations include three kinds: solid state,[10] solution,[11] and solvent mediation.[12] The solvent-mediated transformation between CPs is rarely reported, owing to the dissolve-recrystallize process of crystals,[13] which commonly induces significant changes in structures and properties of CPs.[14] Dong and co-workers studied an irreversible transformation from a 3D Cu^{+} framework to a 1D Cu^{2+} chain induced by oxygen and methanol medium.[15] Our group presented a systematic investigation on the interconversions among four cobalt complexes by mediating the DMF/H_2O volume ratios.[16] Solid-state single-crystal-to-single-crystal (SCSC) transformation among CPs is also scarcely observed because the single crystallinity is hardly retained during conversion, particularly in the solid phase.[17] Some CPs have been obtained via this method, however, they were inaccessible through traditional synthesis method.[18] Several typical characteristics with regard to dynamic responsive phenomena would appear along with structural transformation, such as: framework flexibility due to the release/inclusion of small molecules and framework rearrangement by cleavage and formation of coordination bonds.[19] Zhang et al. found that the transformation triggered by reversible dehydration-rehydration causes a unique accordion-like contraction-expansion movement of the crystal lattice along the *c* axis with the unit cell shortening as much as 24%.[20] Chen et al. reported a drastic rearrangement involving cleavage and formation of coordination bonds in a 3D framework, which increased the degree of interpenetration from five- to six-fold.[21]

Although the structural transformation has been adopted in some degree to synthesize new complexes, the investigations of transition coupled with solvent-mediated and solid-state in a system of nickel-based CPs remain unexplored.[2] Herein, we used 2-(4-carboxybenzoyl)benzoic (H_2cbb) and 4,4′-bipyridine (bipy) mixed ligands and Ni^{2+} ion to construct CPs and observed the interesting structural transformation behaviors. Two temperature-dependent two-dimensional (2D) [Ni(cbb)(bipy)(H_2O)$_2$] (**1**) and [Ni(cbb)(bipy)$_{0.5}$] (**2**) were hydrothermally synthesized and between them two charming solvent-mediated structural transformations existed. According to Ostwald rule of stages,[22] **2** was the thermodynamically stable product whose formation was preceded by the nucleation of the kinetically favored phase of **1**. Remarkably, 2D [Ni(cbb)(bipy)] (**3**) and 3D [Ni(cbb)(bipy)$_{1.5}$]·H_2O (**4**) were accidentally discovered by the thermal decomposition of **1**[23, 24]. Product **3** was the water-removed phase, differing with the original **1** in coordination fashions of carboxylate groups. Moreover, besides cleavage and formation of coordination bonds, a very scarce dynamic responsive feature of the releases of partial cbb^{2-} and bipy ligands was observed in the solid-state SCSC transformation from **3** to **4**.[25] And the transformation

mechanism was firstly proposed. The reasonability of the solvent-mediated and solid-state SCSC transformation mechanisms has also been corroborated by powder X-ray diffraction (PXRD), in-situ variable-temperature powder X-ray diffraction (VTPXRD) and thermogravimetric analyses (TGA), respectively.

Results and Discussion

Materials and General Methods

All solvents and initial materials for synthesis were purchased commercially. Infrared spectra were measured as KBr discs on a Nicolet Avatar 360 FTIR spectrometer. Elemental analyses of C, H, and N were recorded with a Perkin-Elmer 2400C elemental analyzer. Thermogravimetric analyses (TGA) were performed in nitrogen stream on a Netzsch TG209F3 equipment. Powder X-ray diffraction (PXRD) data were all collected on a Bruker D8 ADVANCE X-Ray Powder Diffractometer. Magnetic properties were obtained on a Quantum Design MPMS-XL-7 SQUID magnetometer. Single Crystal Diffraction data were collected on a Bruker-AXS SMART CCD area detector diffractometer equipped with Mo-Kα radiation (λ = 0.71073 Å) at 293 K. Owing to CP **3** is transient and unstable, a lot of colourless enamel was smeared onto the surface of single crystal of **3** to complete X-ray experiments. The final formulas were determined by combining single crystal structures, elemental microanalyses, and TGA data. Partial crystallographic data and structure refinement results are listed in Table 1. Selected bond length/angle data are showed in Table S1†. The mutual conversions of **1-4** are showed in Scheme 1. The various transformation studies are given in Table 2. The solid state and solvent mediated transformation studies have been carried out in 10 mL beaker and hydrothermal reaction vessels with a capacity of 10 mL, respectively.

Table 1. Crystallographic Data of **1-4**

	1	2	3	4
formula	$C_{25}H_{20}N_2NiO_7$	$C_{20}H_{12}NNiO_5$	$C_{25}H_{16}N_2NiO_5$	$C_{30}H_{20}N_3NiO_6$
*M*r	519.12	405.02	483.11	577.20
crystal system	Monoclinic	triclinic	Monoclinic	Monoclinic
space group	*Cc*	$P\bar{1}$	*Cc*	*C*2/*c*
a (Å)	9.765	9.406	9.884	15.331
b (Å)	17.154	9.512	18.292	33.860
c (Å)	14.568	11.655	13.049	10.827
α (deg)	90	75.58	90	90
β (deg)	103.06	80.95	102.75	104.23
γ (deg)	90	66.33	90	90
V (Å^3)	2377.2	923.2	2301.3	5447.5
Z	4	2	4	8
D_{calc}(g cm^{-3})	1.451	1.457	1.395	1.408
F(000)	1072	414	992	2376
R_{int}	0.0170	0.0287	0.0331	0.0212
GOF on F^2	1.044	1.066	1.007	1.047
$R1^a$ [I>2σ(I)]	0.0476	0.0874	0.0657	0.0553
$wR2^b$ (all data)	0.1758	0.3773	0.1768	0.2238

$^aR_1=\Sigma||F_o|-|F_c||/\Sigma|F_o|; wR_2=[\Sigma w(F_o^2-F_c^2)^2/\Sigma w(F_o^2)^2]^{1/2}$.

Scheme 1. The mutual conversions of **1-4**

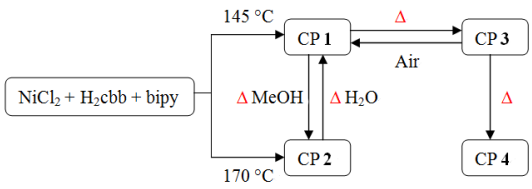

Synthesis of [Ni(cbb)(bipy)(H$_2$O)$_2$] (1)

$NiCl_2{\cdot}6H_2O$ (0.0118 g, 0.05 mmol) was dissolved in distilled water (10 mL), then added $H_2cbb{\cdot}H_2O$ (0.0135 g, 0.05 mmol), bipy (0.0078 g, 0.05 mmol) and two drops of KOH solution (0.025 mol/L). The mixture was stirred vigorously for 30 min and then heated at 145 °C for 72 h. Blue block-shaped crystals were obtained, yielding in 64%. Elemental analysis calcd. (found.) for $C_{25}H_{20}N_2NiO_7$: C, 57.84 (57.71); H, 3.88 (3.93); N, 5.40 (5.29). IR data (KBr, cm^{-1}): 3600 m, 3296 m, 3195 m, 3041 m, 2211 w, 1660 s, 1609 s, 1388 s, 1288 s, 1224 w,1131 w, 1065 w, 937 m, 822 s, 729 s, 680 w, 630 w, 515 w.

Synthesis of [Ni(cbb)(bipy)$_{0.5}$] (2)

$NiCl_2{\cdot}6H_2O$ (0.0118 g, 0.05 mmol) was dissolved in distilled water (10 mL), then added $H_2cbb{\cdot}H_2O$ (0.0135 g, 0.05 mmol), bipy (0.0039 g, 0.025 mmol) and two drops of KOH solution (0.025 mol/L). The mixture was stirred vigorously for 30 min and then heated at 170 °C for 72 h. Green block-shaped crystals were afforded with yield of 56%. Additionally, crystals of **2** could also be constructed with a similar ratio of reactants as that of **1** at 170 °C. Elemental analysis calcd. (found.) for $C_{20}H_{12}NNiO_5$: C, 59.31 (59.44); H, 2.99 (2.78); N, 3.46 (3.55). IR data (KBr, cm^{-1}): 3435 w, 3062 w, 1667 m, 1588 m, 1524 s, 1288 m, 1238 m, 1145 w, 944 w, 859 m, 795 w, 729 m, 508 w, 451 w.

Table 2. Details of the Transformation Studies

	reactant	mode	product	color	T/°C	t/h
1 to **2**	**1**	MeOH-medium	**1&2**/crystal	blue to green	170	48
1 to **2**	**1**	MeOH -medium	**2**/crystal	blue to green	170	72
1 to **2**	**1**	other-medium	**2**/powder	blue to green	170	72
2 to **1**	**2**	water-medium	**2**/crystal	---	145	72
2 to **1**	**2**	other-medium	**2**/crystal	---	145	72
2 to **1**	**2&bipy** (1:1)	water-medium	**1**/ powder	green to blue	145	72
2 to **1**	**2&bipy** (1:1)	other-medium	**2**/ powder	---	145	72
1 to **3**	**1**	solid state (Δ)	**3**/ crystal	blue to green	120-290	<0.5
3 to **4**	**3**	solid state (Δ)	**4**/ crystal	green to black	300-330	<0.3
4 to **1/3**	**4**	solvent-medium	**4**/ crystal	---	145-170	72
4 to **1/3**	**4&cbb& bipy(2:2:1)**	solvent-medium	**4**/ powder	---	145-170	72

Conversion of 1 into 2

The crystals of **1** (10 mg) were immersed in methanol and then activated at 170 °C for 72 h to afford **2** (42%).

Conversion of 2 into 1

The crystals of **2** and bipy ligand were mixed and immersed in water and then activated at 145 °C for 72 h. Some blue crystals of **1** were afforded.

Conversion of 1 into [Ni(cbb)(bipy)] (3) and [Ni(cbb)(bipy)$_{1.5}$]·H$_2$O (4)

The product **1** (10 mg) was carefully placed into a crucible under nitrogen atmosphere and heated at 250 °C for 3 h. Green block-shaped crystals of **3** (93%) were obtained. While the intermediate **3** was further heated at 330 °C for 3 h, slant black block-shaped crystals of **4** (60%) were formed. Furthermore, all of our attempts to synthesize **3** directly were unsuccessful,

while the synthesis of **4** has been reported by Xu et al..[23] Elemental analysis and IR data for Crystals of **3** were not collected since phase **3** is transient and unstable. Elemental analysis calcd. (found.) for $C_{30}H_{22}N_3NiO_6$ (**4**): C, 62.21 (62.08); H, 3.83 (3.92); N, 7.25 (7.12). IR data (KBr, cm^{-1}) for **4**: 3741 w, 3390 w, 3058 w, 1654 m, 1602 s, 1538 s, 1400 s, 1273 m, 1070 w, 1012 w, 930 w, 814 w, 721 m, 633 w, 509 w.

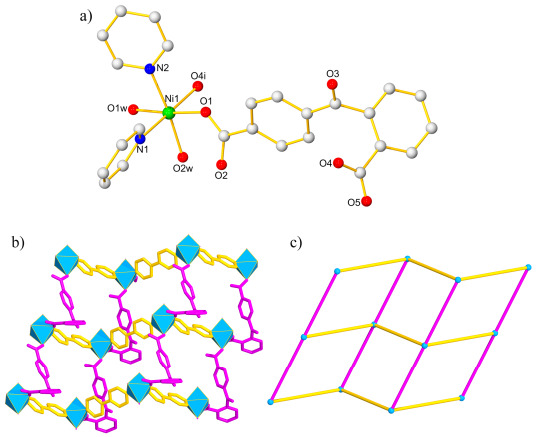

Fig. 1 a) The coordination environment of Ni^{2+} ion in **1**. Symmetry code: (i) 1 + x, y, z. b) View of the 2D wavelike layer structure parallel to *ac* crystal face in **1**. c) The topology of 2D sheet in **1**.

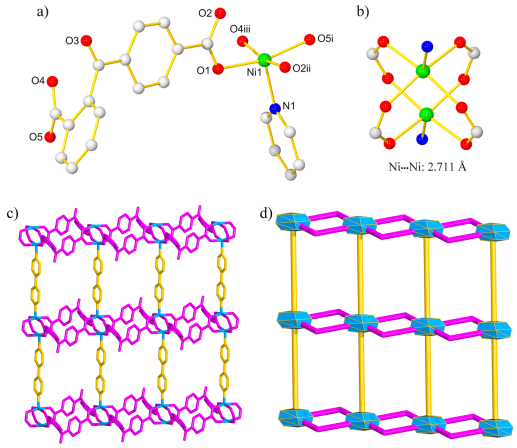

Fig. 2 a) The coordination environment of Ni^{2+} ion in **2**. Symmetry codes: (i) 2 - x, 2 - y, 1 - z; (ii) x, 1 + y, z; (iii) 2 - x, 1 - y, 1 - z. b) A binuclear Ni^{2+} ions arrangement in **2** showing a typical paddle wheel motif with the Ni···Ni distance of 2.711 Å. c) View of the 2D layer structure in **2**. d) The simplified structure of 2D sheet in **2**.

Crystal Structure of [Ni(cbb)(bipy)(H_2O)$_2$] (1)

Single-crystal X-ray crystallography study shows that product **1** crystallizes in the monoclinic system with *Cc* space group. The asymmetric unit contains one Ni^{2+} ion, one deprotonated cbb^{2-}, one bipy and two water ligands. As shown in Fig. 1a, the Ni^{2+} ion is octahedrally coordinated by two nitrogen atoms from two bipy, two carboxylate oxygen atoms from two cbb^{2-} and two water molecules. Adjacent Ni^{2+} ions are bridged by bipy (Ni···Ni, 11.273 Å) to form 1D zig-zag chains along the *c* axis, which are further linked by cbb^{2-} to produce a 2D wavelike 4^4 grid layer parallel to the *ac* crystal face (Fig. 1b,1c).

Crystal Structure of [Ni(cbb)(bipy)$_{0.5}$] (2)

Product **2** crystallizes in the triclinic system, $P\bar{1}$ space group, and features a paddle-wheel dinuclear-based 2D grid. The asymmetric unit consists of one Ni^{2+} ion, one deprotonated cbb^{2-} and half a bipy (Fig. 2a). Ni^{2+} ion adopts a distorted square-pyramidal geometry with four carboxylate oxygen atoms from four cbb^{2-} in the equator plane and pyridyl nitrogen atom of bipy in the axial position. Two centrosymmetric Ni^{2+} ions are bridged by four carboxyl groups in bidentate fashions to give a paddle-wheel shaped dimer (Ni···Ni = 2.711 Å) (Fig. 2b) in which the axial sites are occupied by two nitrogen atoms from two bipy. These dimers are connected by cbb^{2-} to form 1D loop chains which are further linked by bipy to afford a 2D layer (Fig. 2c-2d).

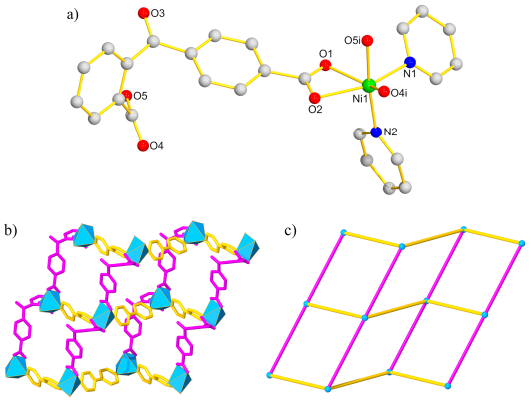

Fig. 3 a) The coordination environment of Ni^{2+} ion in **3**. Symmetry code: (i) 1 + x, y, z. b) View of the 2D wavelike layer structure in **3**. c) The topology of 2D sheet in **3**.

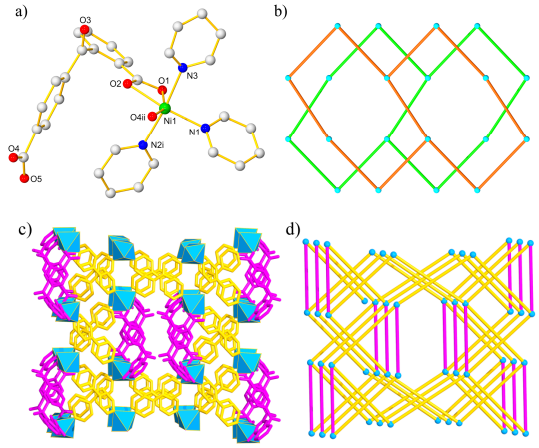

Fig. 4 a) View of the coordination environment of Ni^{2+} ion in **4**. Symmetry code: (i) 0.5 + x, 0.5 - y, 0.5 + z; (ii) 2 - x, y, 1.5 - z. b) 2D 3^6 layers with a dislocated interlayer configuration in **4**. c) View of the 3D net in **4**. d) The simplified structure of **4**.

Crystal Structure of [Ni(cbb)(bipy)] (3)

Product **3** is in the monoclinic system with *Cc* space group (Fig. 3a). The main structural feature of **3** is almost identical with that of **1** (Fig. 3b-3c). Differently, *p*- and *o*-carboxyl groups both employ bidentate chelating modes in **3** instead of monodentate modes in **1**. Additionally, some structural parameters change slightly: the dihedral angle between two phenyl rings in cbb^{2-} is 69.44° (**1**: 65.07°); the dihedral angles between *p*-, *o*-carboxyl groups and their attached phenyl rings are 10.43° and 52.14°, respectively (**1**: 31.20°, 21.19°, respectively); the bond lengths of Ni-N fall in 2.046-2.097 Å (**1**:

2.084-2.099 Å); the Ni-O distances are in the range of 2.079-2.201 Å (**1**: 2.043-2.061 Å) (Table S1†).

Crystal Structure of $[Ni(cbb)(bipy)_{1.5}]\cdot H_2O$ (4)

Though CP **4** has been roported by Xu et al., the structure of **4** is described here in order to help understand clearly.[23] **4** is in the monoclinic system with *C2/c* space group. The asymmetric unit contains one Ni^{2+} ion, one deprotonated cbb^{2-}, one and a half bipy and one lattice water molecule. As shown in Fig. 4a, the Ni^{2+} ion exhibits a distorted octahedral geometry, defined by three oxygen atoms from two cbb^{2-} and three nitrogen atoms from three bipy. The *p*- and *o*-carboxyl groups of cbb^{2-} exhibit monodentate and bidentate chelating modes, respectively. The Ni^{2+} ions are connected by bipy to form 2D 3^6 layers with a dislocated interlayer configuration (Fig. 4b). In addition, adjacent Ni^{2+} ions are connected by cbb^{2-} to give rise to loop units which exhibit out-of-plane connectivity to link the adjacent layers to generate a 3D structure (Fig. 4c-4d).

Solvent-Mediated Structural Transformations

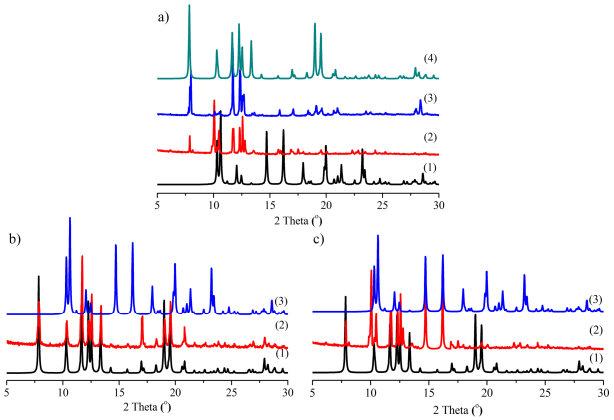

Fig. 5 View of the solvent-mediated transformations of **1** and **2**. a) The methanol-mediated transformation of **1** to **2**: PXRD patterns of as-simulated **1** (1), the activation of **1** in methanol at 170 °C for 48 h (2) and 72 h (3), and as-simulated **2** (4). b-c) The water-mediated transformation of **2** to **1** under the condition of adding bipy ligand: PXRD patterns of as-simulated **2** (1), the activation of **2** (b2) / **2&bipy** (c2) at 145 °C in water and as-simulated **1** (3).

During the initial synthesis from Ni^{2+} ions, H_2cbb and bipy reactant systems at 145 °C, blue crystals of **1** were obtained which showed heavily twinned rosettes. While trying to improve the quality of **1** through tuning the reaction temperature, new green crystals of **2** were gained at 170 °C, which are recognized easily due to different colours and morphologies with **1** (Fig. S1). This observation prompted us to explore the relation between **1** and **2** by further experiments. Sample **1** was soaked in water and various organic solvents in a vessel and then activated at 170 °C. Fortunately, green block-shaped crystals were afforded faultlessly through methanol mediation, which were chemically and structurally identical with crystals of **2**, as evidenced by single-crystal diffraction and PXRD (Fig. S2). The methanol-mediated conversion from **1** to **2** was gradually completed over time. When **1** was activated for 48 h and 72 h, the products correspond to a mixture of **1** and **2**, and only **2**, respectively (Fig. 5a). Analogously, sample **2** was immersed into water and various organic solvents and then activated at 145 °C for 72 h. PXRD patterns revealed that transformation from **2** to **1** failed as crystals of **2** maintained optical transparencies and their single crystal integrity (Fig. 5b, S3a), which could be forecasted since **2** is lack of free bipy by comparing the formulae of **1** and **2**. However, when sample **2** and bipy ligand were mixed according to the ratio of 1:1 and immersed into water and various organic solvents and then activated at the synthesized conditions of **1** (145 °C for 72 h), some blue crystals were just obtained in water mediation. And the PXRD experments were performed to attest the transformation from **2** to **1** under the condition of adding bipy ligand (Fig. 5c, S3b).

These results show that **1** could undergo methanol-mediated transformation to afford **2** and **2** might convert to **1** under the condition of adding bipy. According to Ostwald rule of stages,[22] crystallization in solutions often starts from the least stable phase, followed by transformation into the thermodynamically more stable species owing to its lowest solubility. Therefore, CP **2** is the thermodynamically stable product whose formation is preceded by the nucleation of the kinetically favored species **1**.[26]

Solid-State SCSC Structural Transformations

CP **1** contains two coordinated water molecules in the asymmetric unit. Thus, investigation on the dehydrated phase is indispensable as it would reveal the dynamics triggered by the release of water molecule. Fortunately, water-free phase **3** was established with the color changes of crystals from blue to green in the range of 120-290 °C, and the conversion was completed gradually with increasing temperature. More strikingly, when **3** was further heated above 300 °C, black blocky product of **4** was obtained (Fig. S1) which showed different ratio of Ni/cbb^{2-}/bipy components with **1** and **3** in the asymmetric unit.

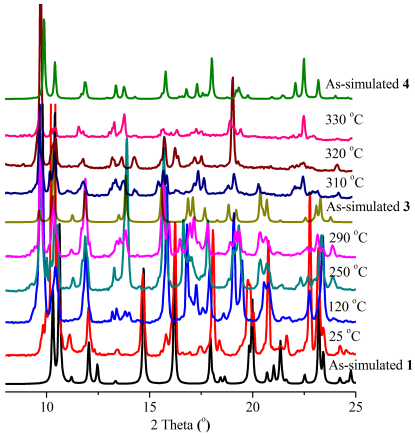

Fig. 6 View of the in-situ VTPXRD patterns showing the multistep transformations of **1** to **3** and **3** to **4**.

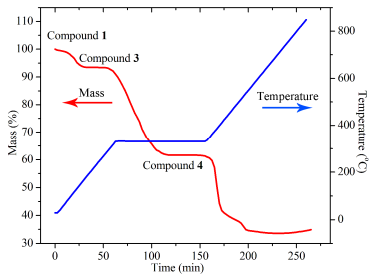

Fig. 7 View of the TGA curve showing the multistep transformations of **1** to **3** and **3** to **4**.

The multistep conversions from **1** to **3** and **3** to **4** can be well demonstrated by in-situ VTPXRD and TGA. The sample was carefully placed over a tantalum heating strip and heated in an atmosphere of dry nitrogen up to 330 °C to recorded in-situ VTPXRD. Data were collected over an angular range of 5-50 (2θ) with a resolution of 0.01° at 1.00 s/step. As shown in VTPXRD (Fig. 6), the overall framework integrity of **1** is retained below 100 °C at which **3** starts to appear. Complete structural transformation from **1** to **3** is reached at 200 °C, and **3** remains crystalline up to 290 °C. Nextly, the intermediate **3** converts to another crystalline phase **4** at 300 °C, and pure crystals of **4** are obtained around 330 °C. Furthermore, TGA were carried out in nitrogen stream at a heating rate of 5 °C/min and heated up to 330 °C and kept for 90 min, then continued to heat up to 800 °C at a rate of 5 °C/min. **1** shows a preliminary weight loss of 6.6% (calc. 6.9%) below 190 °C, corresponding to the elimination of water molecules and indicating the formation of **3**. In the constant temperature area of 330 °C, an observed weight loss of 31.4% agrees well with the dissociation of 1/2cbb^{2-} and 1/4bipy (calc. 33.6%), which implies the generation of **4**. The sample weight is almost invariable during the second half of the constant temperature of 330 °C, revealing the stability of **4**. The framework of **4** is decomposed rapidly above 350 °C (Fig. 7). Additionally, TGA of **H_2cbb&bipy (2:1)** exhibits a sharp weight loss in the range of 100-500 °C, which confirms the dissociation of 1/2cbb^{2-} and 1/4bipy accompanying the transitions of **3** to **4** at 330 °C (Fig. S4). Based on these results, three chemical equations concerning the transformations of **1** to **3** and **3** to **4** could be introduced:

$$[Ni(cbb)(bipy)(H_2O)_2](\mathbf{1}) \xrightarrow{\Delta} [Ni(cbb)(bipy)](\mathbf{3}) + 2H_2O \quad (1)$$

$$[Ni(cbb)(bipy)](\mathbf{3}) \xrightarrow{\Delta} 1/2[Ni(cbb)(bipy)_{3/2}](\mathbf{3'}) + 1/2cbb + 1/4bipy + 1/2Ni \quad (2)$$

$$[Ni(cbb)(bipy)_{3/2}](\mathbf{3'}) + H_2O \xrightarrow{Air} [Ni(cbb)(bipy)_{3/2}]\cdot H_2O(\mathbf{4}) \quad (3)$$

The above results establish that transformations from **1** to **3** and **3** to **4** are multistep sequential transitions triggered by the removal of coordinated water and partial organic ligands, respectively. Product **3** acting as an intermediate can be considered as an "···ABAB···" packing style. And a possible pathway involving three different steps is proposed to demonstrate the process of the transitions among the three phases (Fig. 8-9). In the first step, the removal of water molecules in **1** allows carboxylate groups to adapt bidentate chelating modes to bridge Ni^{2+} ions to form a 2D layer (CP **3**). Meanwhile, a contraction-expansion or breathing-like movement was exhibited (Fig. 8). In the second step, the Ni-O(*p*-) bonds in "A" layer of **3** are broken under external heat stimuli, leading to the creation of 1D chains dangling monocoordinated bipy, between which relative slipping takes place simultaneously. At this moment, cbb^{2-} revolves voluntarily and chooses adjacent Ni to bond to form a loop. Notably, there are vacant sites (red dashed) in the Ni^{2+} centers. In "B" layer, the influence of thermal movement is so severe that all coordination bonds around the Ni^{2+} ions in **3** are destroyed and both of cbb^{2-} and bipy are dissociative. In the final step, as partial bipy in "B" layer and the free sites of Ni^{2+} ions in "A" layer are already close and self-adjust in suitable orientation, bonding reaction is facilitated with ease.[27] While other dissociative organic ligands (1/2cbb^{2-} and 1/4bipy) are decomposed under thermal shock. These changes noted above lead to the formation of product **4** (Fig. 9).

The pathways outlined above for the multistep transformations among **1**, **3** and **4** are very rarely documented.[27] It not only discloses a possible clue to what would happen in the three CPs during the process of heating, but also proposes a possible model for such transformations.

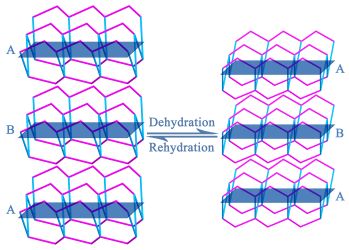

Fig. 8 The solid-state reversible SCSC conversion of **1** to **3**: a contraction-expansion cycle of a 2D layered structure was exhibited in the dehydration-rehydration process.

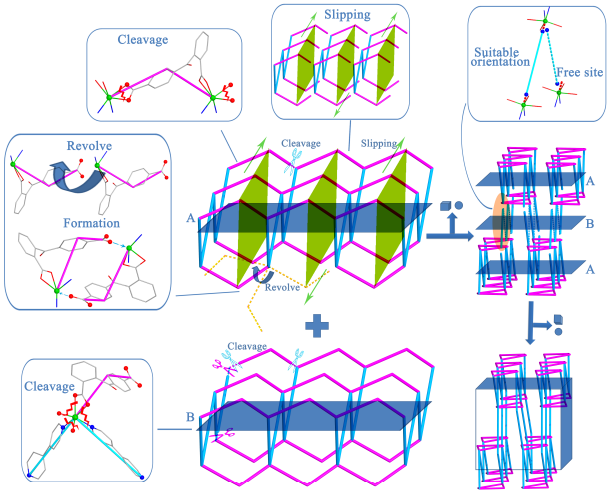

Fig. 9 A possible mechanism for the solid-state SCSC conversion of **3** to **4**. The structural reorganization in "A" layer of **3**: triggered by cleavage of bonds, slipping of chains, revolve of cbb^{2-} and formation of new bonds. The structural reorganization in "B" layer of **3**: all bonds linking with Ni^{2+} ions are destroyed, cbb^{2-} and partial bipy are decomposed in small gaseous fragments, while the metal Ni keep in solid state in the residue (: small gaseous fragments).

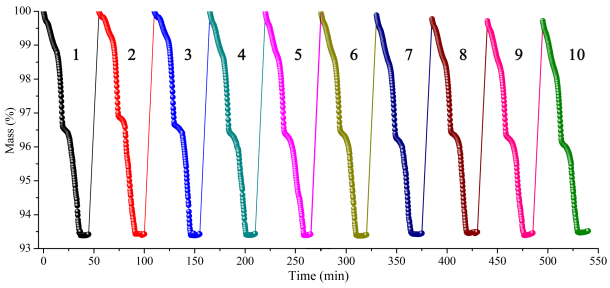

Fig. 10 Ten cycles of the reversible water uptake accompanying the transformation between **1** and **3**, showed by the TGA curves.

Interstingly, the dehydrated phase **3** was transient and unstable, reverting back to the more stable product of **1** rapidly upon exposing sample **3** in air (Fig. S5). The driving force of the structural transformation from **3** to **1** can be attributed to the increase of Ni-O bond lengthes in **3** (**1**: 2.043-2.061 Å; **3**: 2.079-2.201 Å), as well as the easy coordination of water molecules.[28] This observation prompted us to examine the recyclability of the dehydration-rehydration process during the transformation. The sample **1** was taken in crucible and heated

to 220 °C for complete dehydration in an atmosphere of flowing dry nitrogen using a heating rate of 5 °C/min. Then the sample was cooled slowly to room temperature and air stream was introduced into the system for rehydration for 10 min. During this process, the sample reabsorbed the water molecules and reached to the initial weight. This process of dehydration-rehydration was repeated ten times, and TGA confirmed the excellent recyclability (Fig. 10). A PXRD investigation on the rehydrated sample also corroborated the integrity of the sample (Fig. S6). This rapid response and recyclable characteristics are desired for environmentally sensing applications of moisture, and the associated color change is suitable for the identification and monitoring of the state of targeted system.

Furthermore, in order to fulfill the conversion from **4** to **3** or **1**, only **4** and **4&cbb& bipy (2:2:1)** were immersed into water and various organic solvents and then activated at 145-170 °C for 72 h, respectively. PXRD patterns revealed that transformation from **4** to **3** or **1** didn't implement since the framework has been partially destroyed under thermal shock (Fig. S7).

Magnetic Properties

The variable-temperature magnetic susceptibilities (χ_M) of **1**, **2** and **4** (**3** is unstable) were measured in the range of 1.8-300 K under 1 kOe to explore the influence of the stuctural conversion on properties. The plots of $\chi_M T$ and $1/\chi_M$ versus T are shown in Fig. 11. They all suggest antiferromagnetic interaction between the Ni^{2+} centers, while the values ($\chi_M T$ and $1/\chi_M$) and the variation trend ($\chi_M T$ vs T and $1/\chi_M$ vs T) show obvious differences.

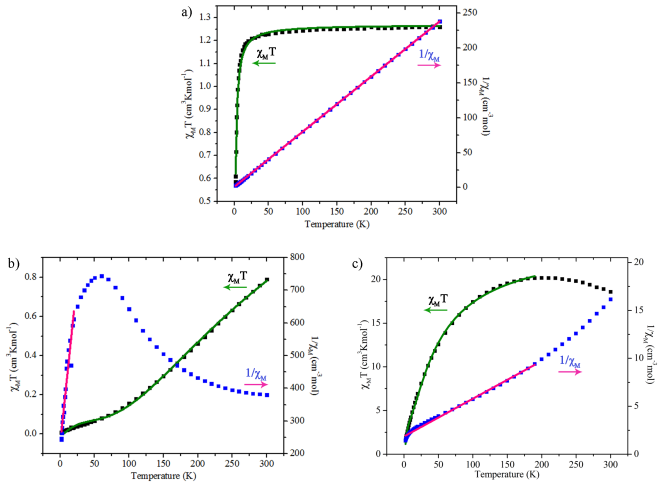

Fig. 11 Temperature variation of the magnetic susceptibility of **1** (a), **2** (b) and **4** (c) in the form of $\chi_M T$ and $1/\chi_M$ vs T.

For **1**, the $\chi_M T$ value at 300 K is 1.26 $cm^3 \cdot K \cdot mol^{-1}$, which is close to the expected spin-only value of 1.21 $cm^3 \cdot K \cdot mol^{-1}$ for one isolated Ni^{2+} ion with $S = 1$ and $g = 2.2$.[29] Upon cooling, the $\chi_M T$ product decreases smoothly until the temperature reduces to 30 K, then $\chi_M T$ falls abruptly and reaches 0.58 $cm^3 \cdot K \cdot mol^{-1}$ at 1.8 K. The continuous decline of $\chi_M T$ upon cooling suggests antiferromagnetic interaction between the Ni^{2+} centers, which is transmitted through cbb^{2-} and bipy bridges. For **2**, the $\chi_M T$ value at 300 K is 0.79 $cm^3 \cdot K \cdot mol^{-1}$, which is lower than the expected value of 1.21 $cm^3 \cdot K \cdot mol^{-1}$ for one spin-only Ni^{2+} center.[29] With temperature falling, $\chi_M T$ is monotonic decreasing, suggesting dominant antiferromagnetic interaction between the Ni^{2+} centers. The $Ni^{2+}\cdots Ni^{2+}$ distance in the dinuclear unit is 2.711 Å, while the nearest $Ni^{2+}\cdots Ni^{2+}$ separations between the adjacent dimers bridged by cbb^{2-} and bipy are 9.212 and 11.125 Å, respectively. So the efficient magnetic exchange interaction is mainly transmitted through the four carboxyl bridges in the paddle-wheel units. The χ_M data of **1** and **2** both can be analyzed by a dinuclear Ni^{2+} system ($S_1 = S_2 = 1$) based on the Hamiltonian $H = -J\sum S_1 S_2$.[30] The χ_M expression is provided in the eq (4) and (5).

$$\chi = \frac{2Ng^2\beta^2}{kT}\frac{e^{2J/kT}+5e^{6J/kT}}{1+3e^{2J/kT}+5e^{6J/kT}} + \rho \quad (4)$$

$$\chi_M = \frac{\chi}{1-(zJ'/Ng^2\beta^2)\chi} \quad (5)$$

The best fitting parameters are obtained as follows. For **1**: g = 2.06, J = -5.24 cm^{-1}, zJ' = -0.04 cm^{-1}, ρ = 0, $R = 1.28 \times 10^{-4}$. And for **2**: g = 2.00, J = -175.24 cm^{-1}, zJ' = -3.70 cm^{-1}, ρ = 0.13%, $R = 1.14 \times 10^{-4}$ ($R = [\sum(\chi_{obs}T-\chi_{calc}T)^2/\sum(\chi_{obs}T)^2]$). The negative J values further indicate the antiferromagnetic coupling between the adjacent Ni^{2+} centers. The plot of $1/\chi_M$ versus T for **1** obeys the Curie-Weiss law, $\chi_M = C/(T-\theta)$, with a Curie constant C = 1.27 $cm^3 \cdot K \cdot mol^{-1}$ and a negative Weiss constant θ = -1.47 K. While upon cooling, $1/\chi_M$ for **2** increases gradually with a distinct plateau (744.45 $cm^{-3} \cdot mol$) appearing below 60 K. Above 20 K, the $1/\chi_M$ versus T plot obeys the Curie-Weiss law with C = 0.05 $cm^3 \cdot K \cdot mol^{-1}$ and θ = -11.31 K.

For **4**, the $\chi_M T$ value at 300 K is 18.58 $cm^3 \cdot K \cdot mol^{-1}$, which is much higher than the expected spin-only value of 1.21 $cm^3 \cdot K \cdot mol^{-1}$ for one isolated Ni^{2+} ion with $S = 1$ and $g = 2.2$. Upon cooling, the $\chi_M T$ product increases smoothly until 20.17 $cm^3 \cdot K \cdot mol^{-1}$ at 200 K, then $\chi_M T$ decreases to a minimum value of 1.55 $cm^3 \cdot K \cdot mol^{-1}$ at 1.8 K. Fitting $1/\chi_M$ below 200 K the Curie-Weiss law yielded gives to θ = -47.21 K and C = 25.40 $cm^3 \cdot K \cdot mol^{-1}$. The negative Weiss constant indicates an obvious intra molecular antiferromagnetic interaction between adjacent Ni^{2+} ions through cbb^{2-} and bipy bridges. The strength of the antiferromagnetic exchange interaction and the spin-orbit coupling for Ni^{2+} were estimated based on eq (6).

$$\chi_M = A\exp(-E_1/kT) + B\exp(-E_2/kT) \quad (6)$$

where $A + B$ equals the curie constant. The E_1 and E_2 are the spin-orbit coupling constant and activation energy of antiferromagnetic interactions, respectively. The best fitting gave: E_1/k = 3.53 K, E_2/k = 46.90 K, A = 5.81 $cm^3 \cdot K \cdot mol^{-1}$, B = 18.80 $cm^3 \cdot K \cdot mol^{-1}$. The value for $A + B$ (24.61 $cm^3 \cdot K \cdot mol^{-1}$) is consistent with the Curie constant of C = 25.40 according to the Curie-Weiss Law. The value for E_1/k is accordant with those given in the literature for both the effects of spin-orbit coupling and site distortion, and the value E_2/k corresponding to spin coupling between the Ni^{2+}, shows the distinct antiferromagnetic exchange mediated between Ni^{2+} through the cbb^{2-} and bipy bridges.[31]

Conclusions

In conclusion, four nickel-based CPs have been prepared, in which the solvent-mediated and solid-state SCSC structural transformations have been observed and studied systematically. Two interesting solvent-mediated conversions were existed between **1** and **2** which are distinct in color, morphology and magnetic property. The solid-state SCSC transformations from **1** to **3** and **3** to **4** correspond to multistep sequential release of coordinated water and partial organic ligands, respectively. Study of solvent-mediated conversions indicates that the self-assembly and the transitions of CPs are related intimately to kinetic and thermodynamic active factors during the

crystallization process. While investigation of solid-state SCSC transformations reveal that the removal of coordinated solvents and partial organic ligands acting as a scarce dynamic responsive feature would accompany structural reorganization. The structural transitions studied herein not only may be considered as simple reorganization reactions, but also propose possible models for such transformations. Additionally, the rapid response and recyclable characteristics observed in the reversible transformation of **1** and **3** can broaden their application in the sensors of moisture.

Acknowledgements

We are grateful for financial support from the NSF of China (Grants 21371142, 20931005, 91022004, 21201139 and 21001088) and the NSF of Shaanxi, China (Grants 2013JQ2016, 2013KJXX-26, 13JS114 and 2014JQ2049).

Notes and references

Key Laboratory of Synthetic and Natural Functional Molecule Chemistry of the Ministry of Education, Shaanxi Key Laboratory of Physico-Inorganic Chemistry, College of Chemistry & Materials Science, Northwest University, Xi'an 710069, P. R. China. E-mail: wyaoyu@nwu.edu.cn.

† Electronic Supplementary Information (ESI) available: Images of single-crystals, additional PXRD patterns, IR, TGA, bond length/angle tables. CCDC 998927 (**1**), 998928 (**2**), 998929 (**3**) and 998926 (**4**). For ESI and crystallographic data in CIF or other electronic format see DOI: 10.1039/b000000x/.

1 (a) C.-M. Wang, T.-Y. Chang, C.-W. Chiu, H.-M. Lin and K.-H. Lii, *Inorg. Chem.*, 2014, **53**, 3266; (b) F. Zhang, Z. Li, T. Ge, H. Yao, G. Li, H. Lu and Y. Zhu, *Inorg. Chem.*, 2010, **49**, 3776; (c) R. Peng, M. Li and D. Li, *Coord. Chem. Rev.*, 2010, **254**, 1.

2 P. Mahata, C.-M. Draznieks, P. Roy and S. Natarajan, *Cryst. Growth Des.*, 2012, **13**, 155.

3 (a) X.-Y. Yi, H.-C. Fang, Z.-G. Gu, Z.-Y. Zhou, Y.-P. Cai, J. Tian and P. K. Thallapally, *Cryst. Growth Des.*, 2011, **11**, 2824; (b) D. J. Lun, G. I. Waterhouse and S. G. Telfer, *J. Am. Chem. Soc.*, 2011, **133**, 5806.

4 M. Nagarathinam, A. Chanthapally, S. H. Lapidus, P. W. Stephens and J. J. Vittal, *Chem. Commun.*, 2012, **48**, 2585.

5 Y.-Q. Lan, H.-L. Jiang, S.-L. Li and Q. Xu, *Inorg. Chem.*, 2012, **51**, 7484.

6 Y. S. Tan, A. L. Sudlow, K. C. Molloy, Y. Morishima, K. Fujisawa, W. J. Jackson, W. Henderson, S. N. B. A. Halim, S. W. Ng and E. R. Tiekink, *Cryst. Growth Des.*, 2013, **13**, 3046.

7 (a) H. Kanoh, A. Kondo, H. Noguchi, H. Kajiro, A. Tohdoh, Y. Hattori, W.-C. Xu, M. Inoue, T. Sugiura and K. Morita, *J. Colloid Interface Sci.*, 2009, **334**, 1; (b) N. Klein, H. C. Hoffmann, A. Cadiau, J. Getzschmann, M. R. Lohe, S. Paasch, T. Heydenreich, K. Adil, I. Senkovska and E. Brunner, *J. Mater. Chem.*, 2012, **22**, 10303.

8 (a) N. Yanai, T. Uemura, M. Inoue, R. Matsuda, T. Fukushima, M. Tsujimoto, S. Isoda, S. Kitagawa, *J. Am. Chem. Soc.* 2012, **134**, 4501; (b) M. R. Warren, T. L. Easun, S. K. Brayshaw, R. J. Deeth, M. W. George, A. L. Johnson, S. Schiffers, S. J. Teat, A. J. Warren, J. E. Warren, *Chem. Eur. J.* 2014, **20**, 5468.

9 D. Yuan, D. Zhao, D. J. Timmons and H.-C. Zhou, *Chem. Sci.*, 2011, **2**, 103.

10 (a) M. J. Katz, T. Ramnial, H.-Z. Yu and D. B. Leznoff, *J. Am. Chem. Soc.*, 2008, **130**, 10662; (b) Z. Niu, J.-G. Ma, W. Shi and P. Cheng, *Chem. Commun.*, 2014, **50**, 1839; (c) X. Bao, P.-H. Guo, J.-L. Liu, J.-D. Leng and M.-L. Tong, *Chem. Eur. J.*, 2011, **17**, 2335.

11 (a) S. K. Ghosh, J. P. Zhang and S. Kitagawa, *Angew. Chem. Int. Ed.*, 2007, **46**, 7965; (b) M.-L. Sun, L. Zhang, Q.-P. Lin, J. Zhang and Y.-G. Yao, *Cryst. Growth Des.*, 2010, **10**, 1464; (c) C. K. Brozek and M. Dincă, *J. Am. Chem. Soc.*, 2013, **135**, 12886; (d) X. Song, T. K. Kim, H. Kim, D. Kim, S. Jeong, H. R. Moon and M. S. Lah, *Chem. Mater.*, 2012, **24**, 3065; (e) S. Jeong, D. Kim, X. Song, M. Choi, N. Park and M. S. Lah, *Chem. Mater.*, 2013, **25**, 1047.

12 (a) C. K. Brozek, L. Bellarosa, T. Soejima, T. V. Clark, N. López and M. Dincă, *Chem. Eur. J.*, 2014, **20**, 6871; (b) J.-J. Zhang, C. S. Day and A. Lachgar, *CrystEngComm*, 2011, **13**, 133; (c) D.-P. Zhang, L.-F. Zhang, G.-L. Li and Z.-H. Ni, *Chem. Commun.*, 2013, **49**, 9582.

13 (a) J. Liu, Y.-X. Tan and J. Zhang, *Cryst. Growth Des.*, 2012, **12**, 5164; (b) V. A. Friese and D. G. Kurth, *Coord. Chem. Rev.*, 2008, **252**, 199.

14 (a) X. Jiang, Z. Li, Y. Zhai, G. Yan, H. Xia and Z. Li, *CrystEngComm*, 2014, **16**, 805; (b) J.-J. Wu, Y.-X. Ye, Y.-Y. Qiu, Z.-P. Qiao, M.-L. Cao and B.-H. Ye, *Inorg. Chem.*, 2013, **52**, 6450; (c) F. Pan, J. Wu, H. Hou and Y. Fan, *Cryst. Growth Des.*, 2010, **10**, 3835.

15 J.-Y. Ge, J.-C. Wang, J.-Y. Cheng, P. Wang, J.-P. Ma, Q.-K. Liu and Y.-B. Dong, *Chem. Commun.*, 2014, **50**, 4434.

16 A.-Y. Fu, Y.-L. Jiang, Y.-Y. Wang, X.-N. Gao, G.-P. Yang, L. Hou and Q.-Z. Shi, *Inorg. Chem.*, 2010, **49**, 5495.

17 (a) J. Li, P. Huang, X.-R. Wu, J. Tao, R.-B. Huang and L.-S. Zheng, *Chem. Sci.*, 2013, **4**, 3232; (b) M. K. Sharma, P. Lama and P. K. Bharadwaj, *Cryst. Growth Des.*, 2011, **11**, 1411.

18 (a) Z. Duan, Y. Zhang, B. Zhang and D. Zhu, *J. Am. Chem. Soc.*, 2009, **131**, 6934; (b) B. Zhang, D. Zhu and Y. Zhang, *Chem. Eur. J.*, 2010, **16**, 9994; (c) F. Wang, Y.-X. Tan, H. Yang, Y. Kang and J. Zhang, *Chem. Commun.*, 2012, **48**, 4842.

19 S. K. Ghosh, W. Kaneko, D. Kiriya, M. Ohba and S. Kitagawa, *Angew. Chem. Int. Ed.*, 2008, **120**, 8975.

20 B. Wei, R. Shang, X. Zhang, X.-D. Shao, Y.-F. Yao, Z.-M. Wang, R.-G. Xiong and W. Zhang, *Chem. Eur. J.*, 2014, **20**, 1.

21 J.-P. Zhang, Y.-Y. Lin, W.-X. Zhang and X.-M. Chen, *J. Am. Chem. Soc.*, 2005, **127**, 14162.

22 W. Ostwald, *Z. Phys. Chem.*, 1897, **22**, 289.

23 During the preparation of this manuscript, we found the direct synthesis and structural description of CP **4** were reported. See: J. Xu, X. Sun, Y. Fan, C. Bi, and M. Sun, *Z. Anorg. Allg. Chem.*, 2012, **638**, 1512.

24 M. Wriedt and C. Näther, *Eur. J. Inorg. Chem.*, 2010, **20**, 3201.

25 (a) S. Wöhlert, T. Runčevski, R. E. Dinnebier, S. G. Ebbinghaus and C. Näther, *Cryst. Growth Des.*, 2014, **14**, 1902; (b) Z. Chen, S. Xiang, D. Zhao and B. Chen, *Cryst. Growth Des.*, 2009, **9**, 5293.

26 L. Carlucci, G. Ciani, J. M. García-Ruiz, M. Moret, D. M. Proserpio and S. Rizzato, *Cryst. Growth Des.*, 2009, **9**, 5024.

27 G. K. Kole and J. J. Vittal, *Chem. Soc. Rev.*, 2013, **42**, 1755.

28 Q. Chen, Z. Chang, W.-C. Song, H. Song, H.-B. Song, T.-L. Hu and X.-H. Bu, *Angew. Chem. Int. Ed.*, 2013, **52**, 11550.

29 W.-H. Yan, S.-S. Bao, J. Huang, M. Ren, X.-L. Sheng, Z.-S. Cai, C.-S. Lu, Q.-J. Meng and L.-M. Zheng, *Dalton Trans.*, 2013, **42**, 8241.

30 (a) A. Roth, A. Buchholz, M. Rudolph, E. Schütze, E. Kothe and W. Plass, *Chem.-Eur. J.*, 2008, **14**, 1571. (b) X. Li, Y. Cai, Z. Fang, L. Wu, B. Wei and S. Lin, *Cryst. Growth Des.*, 2011, **11**, 4517.

31 Y.-P. Li, Y. Chai, G.-P. Yang, H.-H. Miao, L. Cui, Y.-Y. Wang and Q.-Z. Shi, *Dalton Trans.*, 2014, **43**, 10947.

Graphical abstract

Four multi-dimensional nickel coordination polymers (CPs) have been prepared via hydrothermal reaction or structural transformation. **1** could undergo methanol-mediated transformation to afford **2** and **2** might convert to **1** in water under the condition of adding bipy. The conversions from **1** to **3** and **3** to **4** were multistep sequential transitions triggered by heat treatment in the solid state. Moreover, **3** could revert back to **1** quickly upon exposure of **3** in air.